Applied Catalysis B: Environmental 142–143 (2013) 329–336

Contents lists available at SciVerse ScienceDirect

Applied Catalysis B: Environmental

journal homepage: www.elsevier.com/locate/apcatb

Deactivation and regeneration of the supported bimetallic Pd–Pb catalyst in direct oxidative esterification of methacrolein with methanol

Yanyan Diao[a], Pu Yang[a], Ruiyi Yan[a], Li Jiang[a,b], Lei Wang[a], Heng Zhang[a,c], Chunshan Li[a], Zengxi Li[b], Suojiang Zhang[a,*]

[a] Beijing Key Laboratory of Ionic Liquids Clean Process, State Key Laboratory of Multiphase Complex Systems, Institute of Process Engineering, Chinese Academy of Sciences, 100190 Beijing, China
[b] College of Chemistry and Chemical Engineering, University of Chinese Academy of Sciences, 100049 Beijing, China
[c] School of Chemistry and Chemical Engineering, Qufu Normal University, 273165 Qufu, China

ARTICLE INFO

Article history:
Received 8 October 2008
Received in revised form 7 March 2013
Accepted 30 April 2013
Available online 7 May 2013

Keywords:
Oxidative esterification
Pd catalyst
Deactivation
Regeneration

ABSTRACT

The deactivation of the supported bimetallic Pd–Pb catalyst in the repeated runs of direct oxidative esterification of methacrolein with methanol in the atmosphere was investigated. The catalysts before and after stability tests were characterized by X-ray diffraction, transmission electron microscopy, X-ray photoelectron spectroscopy, inductively coupled plasma mass spectrometry, Brunauer–Emmett–Teller method and thermogravimetric analysis. The results indicated that the major factor affecting the deactivation of the catalyst was the deposition of organic substances on the surface active sites of the catalyst during batch reaction. Washing the deactivated catalyst with either MeOH or an aqueous hydrazine solution at 80 °C could completely recover the initial activity of the catalyst, and calcining the deactivated catalyst in air at 500 °C and then reducing in an aqueous hydrazine solution could partly recover its activity. The deactivation and regeneration of the catalyst in the direct oxidative esterification at gas–liquid–solid phase are important and meaningful.

1. Introduction

Methyl methacrylate (MMA) is an important substrate for producing polymer with the characteristics of good transparency and weather resistance for paints and coatings. Today, the global demand for MMA continues to grow, whereas the capacity for the production of MMA is not enough to meet the demand. The acetone cyanohydrine (ACH) process for manufacturing MMA, which was commercialized by Imperial Chemical Industries Ltd. (ICI) in 1930s, was the only industrial process until 1980 [1]. This traditional process producing MMA, uses highly toxic hydrocyanic acid (HCN) as the raw materials, and generates solid waste of ammonium bisulfate and a large amount of acidic wastewater. The ACH process was gradually phased out because of its toxicity, suspected carcinogenicity, and pervasiveness in the environment, especially in groundwater.

Recently, the direct oxidative esterification process for manufacturing MMA has been attracting more and more attention because of its environment-friendly process and its efficiency in utilizing atoms. The direct oxidative esterification process includes two steps. The first step is the oxidation of isobutene to methacrolein (MAL) in the present of oxygen. The second step is the direct oxidative esterification of MAL with methanol (MeOH) to MMA in the present of air (Scheme 1). The direct oxidative esterification process is a new, environmentally friendly method of producing MMA, and it does not generate harmful waste products such as ammonium bisulfate and acidic wastewater. The key factor in this process is the development of excellent catalyst for the direct oxidative esterification of MAL with MeOH in the atmosphere [1,2].

In previous studies, the supported precious metals (Pd, Pt and Au) and bimetallic catalysts (Pd–Ag, Pd–Bi and Pd–Pb) have exhibited relevant activity for the direct oxidative esterification of MAL with MeOH to MMA [3–8]. In the γ-alumina supported bimetallic Pd–Pd catalysts exhibited high activity for the direct oxidative esterification of MAL with MeOH to MMA [5–7]. One of the drawbacks of the supported precious metal catalytic process is the high cost of noble metal, which makes it necessary to prolong the life of the catalyst for the succeeding reactions. The evaluation of catalyst stability is recognized as an integral part of its study, industrial or academic [9–14], because determining the stability of a catalyst is essential to optimize the process conditions and prevent premature catalyst deactivation [15–19].

* Corresponding author. Tel.: +86 10 8262 7080; fax: +86 10 8262 7080.
E-mail address: sjzhang@home.ipe.ac.cn (S. Zhang).

0926-3373/$ – see front matter © 2013 Elsevier B.V. All rights reserved.
http://dx.doi.org/10.1016/j.apcatb.2013.04.064

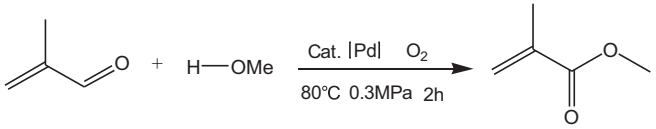

Scheme 1. Pd-catalyzed direct oxidative esterification of MAL with MeOH to MMA.

Catalyst deactivation is one of the important processes in the application of catalyst in chemical industry. In the gas-phase reaction, the general factors of deactivation and premature degradation of supported precious metal catalysts include particle growth of various reasons [20], coke deposition and coke transformation [21], the oxidation of noble metal crystallite and the influence of the support material on the noble metal surface. In the hydrodechlorination reactions of tetrachloroethylene (TTCE), chlorobenzene (CBZ) and dichloromethane (DCM) in the gas phase with Pd/Al_2O_3 as a catalyst, coke formation plays a key role in the deactivation process [22]. In the catalytic combustion of methane to carbon dioxide and water, the Pd-based catalysts were found to sinter [23]. In the selective catalytic reduction of NO_x by methane with Pd/zeolite catalysts, the formation of palladium oxide was detected, the tendency for Pd-agglomeration was found to be promoted by water [24]. In the liquid-phase reaction, the reasons for deactivation mainly include corrosion [25], noble metal leaching because of dissolution [26], blocking of active sites by the deposition of water, and water-soluble and non-water-soluble substances [27], and interaction of the catalyst with the substrates in the reaction mixture. In slurry-phase hydrogenation reactions, the loss of precious metal through the formation of soluble complex compounds occurred. In the catalytic hydrodechlorination (HDC) of tetrachloroethylene (PCE) with the palladium catalyst supported on activated carbon (Pd/C), the deactivation was mainly due to the adsorption of the reaction products on the catalyst [28].

For the important gas–liquid–solid reaction of the direct oxidative esterification of MAL with MeOH in the atmosphere with bimetallic Pd–Pb catalyst, no information regarding the catalyst's deactivation and regeneration has been reported yet. This lack of relevant data prompted us to investigate catalyst deactivation and regeneration in the mentioned process. Generally, there are four theoretically possible reasons for catalyst deactivation: (i) Pd crystallite growth; (ii) the leaching of Pd and Pb; (iii) the oligomerization of MAL and MMA; and (iv) the strong adsorption of other organic substances.

Therefore, it is imperative to investigate the stability of bimetallic Pd–Pb catalyst used in direct oxidative esterification of MAL with MeOH in the atmosphere. In this study, the catalyst's lifespan was investigated with both batch process and continuous-flow process. To analyze the possible contribution of each of the aforementioned phenomena toward catalyst deactivation in batch system, the fresh and deactivated catalysts were characterized by X-ray diffraction (XRD), transmission electron microscopy (TEM), X-ray photoelectron spectroscopy (XPS), inductively coupled plasma mass spectrometry (ICP-MS), Brunauer–Emmett–Teller (BET) method and thermogravimetric analysis (TG). Moreover, the simple reactivation methods of washing the deactivated catalyst with either MeOH or an aqueous hydrazine solution, and calcining the deactivated catalyst in air at 500 °C and then reducing in an aqueous hydrazine solution were evaluated.

2. Experimental

2.1. Catalyst preparation

The catalyst used in the experiments with the loading mass of 5 wt.% Pd and 5 wt.% Pb on $MgO–Al_2O_3$, which was abbreviated as $Pd_5Pb_5/MgO–Al_2O_3$, was prepared according to the procedure mention in the succeeding sections.

2.1.1. Synthesis of $MgO–Al_2O_3$ support

A magnesium acetate aqueous solution was heated to 50–100 °C under constant stirring. A given amount of γ-Al_2O_3 (200–250 μm) was added to the solution. When the water evaporated, the obtained Al_2O_3 with absorbed magnesium acetate was dried in a vacuum at 45 °C for 12 h, and then calcined at 600 °C in air for 3 h. The support of $MgO–Al_2O_3$ (2 wt.% Mg on Al_2O_3) was obtained.

2.1.2. Synthesis of the $Pd_5Pb_5/MgO–Al_2O_3$ catalyst

The $Pd_5Pb_5/MgO–Al_2O_3$ catalyst was prepared by the incipient impregnation of $MgO–Al_2O_3$ with a mixed aqueous solution of palladium chloride and lead acetate at 50–100 °C under stirring for 1 h. After impregnation, a hydrazine aqueous solution was added to the above solution to reduce the Pd and Pb ion adsorbed on the support. After filtration, washing with deionized water, and drying in vacuum at 45 °C for 12 h, the catalyst $Pd_5Pb_5/MgO–Al_2O_3$ was obtained. The catalyst was kept in a vacuum desiccator before use.

2.2. Characterization

Several analytic techniques were applied to characterize the fresh and deactivated catalyst in this study. XRD patterns were obtained with an X'Pert Pro MPD X-ray diffractometer from PANalytical, with Cu Kα radiation (λ = 0.154187 nm) and a scanning angle 2θ from 10° to 90°. TEM analysis was performed with an FEI Tecnai 20 electronic microscope. The specimens for TEM analysis were prepared by dispersing the fresh or deactivated catalyst in ethanol followed by ultrasonic treatment. The samples were deposited onto a holey carbon film supported on a copper grid, and then dried in the atmosphere.

XPS data were obtained with an ESCALab220i-XL electron spectrometer from VG Scientific with the radiation of 300 W Al Kα radiations. The base pressure was about 3×10^{-9} mbar. The binding energies were referenced to the C 1s line at 284.8 eV from the adventitious carbon. The actual Pd contents in the catalyst and in the bulk solution were all determined by the OPTIMA 5300DV inductively coupled plasma-mass emission spectrometry (ICP-MS) manufactured by Perkin-Elmer. The given amount of the catalyst was dissolved in a mixture of hydrochloric acid (HCl) and nitric acid (HNO_3) with the volume ratio of 3:1. The above solution was diluted to the required volume for the analysis and determination of its Pd and Pb contents.

The specific surface area, the pore volume and the pore size distribution were determined based on the N_2 adsorption on the powder, using the Brunauer–Emmett–Teller (BET) method. The measurements were obtained by the Autosorb series ASIMP apparatus from Quantachrome. Before the measurements were obtained, the samples were degassed at 300 °C under vacuum condition for 5 h. TG/DTA analysis was carried out on NETZSCH STA 449C with an air flow of 30 ml min^{-1} and a temperature of 900 °C at a heating rate of 10 °C min^{-1}.

Pyridine-IR was used to determine the different acid sites on the surface $MgO–Al_2O_3$ caused by the different bonded pyridine and their specific absorption bands. The pyridine adsorbed at the Lewis (L-Py) and Brønsted (PyH^+) acid sites exhibits bands at around 1445–1460 and 1540–1548 cm^{-1}, respectively [29,30]. Before the experiment, $MgO–Al_2O_3$ was calcined at 500 °C. Pyridine FTIR spectrum was recorded on a Nicolet 6700 spectrometer equipped with a cell in situ. The sample was pressed into a self-supporting plate (13 mm diameter), placed in an IR cell and treated at 200 °C under vacuum (5.0×10^{-3} Pa) for 1 h. After the IR cell was cooled to room temperature, pyridine vapor was introduced into the cell and adsorbed for 30 min. Then it was scanned after being vacuumed

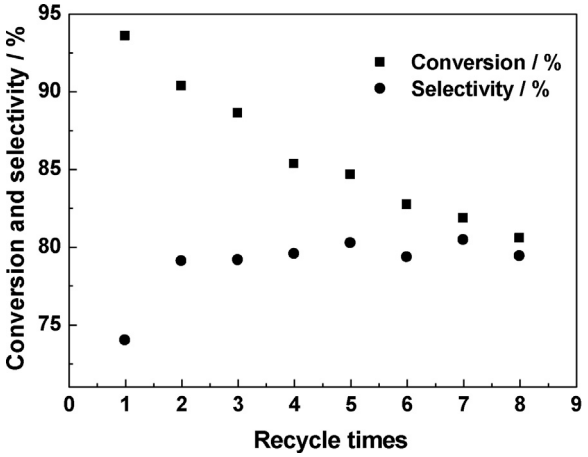

Fig. 1. The degradation of catalyst in the batch process of the direct oxidative esterification of MAL with MeOH in air.

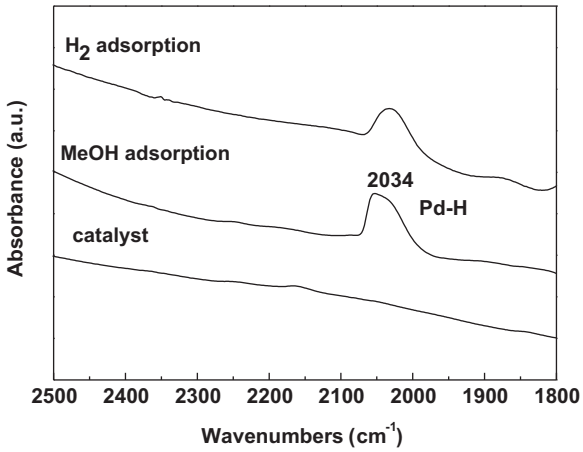

Fig. 2. FTIR spectra of MeOH and H_2 absorbed on catalyst.

for 20 min and recorded at room temperature, 100 °C, 150 °C, and 200 °C under vacuum.

FTIR spectrum of MeOH adsorption was also recorded on a Nicolet 6700 spectrometer equipped with a cell in situ. Before the experiment, MeOH was purified by a frozen pump method with liquid nitrogen. The catalyst was pressed into a self-supporting plate, placed in an IR cell and treated at 200 °C under vacuum for 1 h. After the IR cell was cooled to 80 °C, MeOH vapor was introduced into the cell. Then it was scanned and recorded. The experimental conditions of H_2 adsorption on the catalyst were the same as MeOH adsorption.

2.3. Catalyst activity–stability evaluation

The catalytic batch reactions were carried out by a bench-scale. 2.0 g of the $Pd_5Pb_5/Mg–Al_2O_3$ catalyst, 15 mL of MAL and 60 mL of MeOH were added into a mechanically stirred 100-mL stainless steel reactor (316 L). In addition, 1.0 ml 2 wt.% solution of NaOH in MeOH and 0.1 g solid $Mg(OH)_2$ were also added into the reactor to neutralize the carboxylic acid that would be gradually produced from the reaction and to keep the solution pH at the range value of 6.0–8.0. All reactions were carried out for 2 h with air flow at the pressure of 3 kg cm^{-2}, the temperature at 80 °C, and with a stirring speed of 800 rpm. The air flow rate of 150 mL min^{-1} was set to ensure that the reactions were maintained in the mass-transport-limited regime and to avoid over-oxidation of the catalyst. After the reactions were stopped, the reactor was cooled to room temperature, and then, the excess gas was slowly vented, the products were removed from the reactor. The reactor and catalyst was washed with the reactant MeOH to clear up the residual product that was not completely moved from the reactor, and then fresh reactants of MAL and MeOH were added for new runs to evaluate the stability of the catalysts.

The catalytic continuous-flow reaction was carried out in a flat-bottomed, mechanically stirred 200 mL stainless steel reactor. The regenerated catalyst washed with MeOH was added to the reactor. A mixed solution of MAL and MeOH was continuously fed to the reactor at the flow of 85 mL h^{-1} (the molar ratio of MeOH to MAL was about 8:1) with an air flow of 170 mL min^{-1}, the pressure of 3 kg cm^{-2}, the temperature of 80 °C, and a stirring speed of 600 rpm. In addition, a 2 wt.% solution of NaOH in MeOH was added to keep the mixture's pH at the range of 6.0–8.0. This continuous-flow reaction was carried out for 15 h.

The reaction mixtures were analyzed by GC (Agilent 6890, equipped with a DB-624 capillary column and an FID detector) and GC–MS. The catalytic activities were expressed as conversion rate (X, %) and selectivity (S, %) which were determined by GC using ethanol as the external standard. The parameters are defined as:

$$X\ (\text{mol}\%) = \left(1 - \frac{C_{\text{aldehyde}}}{C_{0\,\text{aldehyde}}}\right) \times 100\%$$

$$S\ (\text{mol}\%) = \left(\frac{C_{\text{ester}}}{C_{0\,\text{aldehyde}} - C_{\text{aldehyde}}}\right) \times 100\%$$

where $C_{0\,\text{aldehyde}}$ is the molar concentration of aldehyde at the beginning of the direct transformation process, C_{aldehyde} is the molar concentration of aldehyde after time t, and C_{ester} is the molar concentration of the corresponding ester after time t.

3. Results and discussion

3.1. Catalyst deactivation in direct oxidative esterification of MAL with MeOH

The direct oxidative esterification of MAL with MeOH in the atmosphere was successfully achieved with $Pd_5Pb_5Mg_2/Al_2O_3$ as the catalyst in the batch process. Fig. 1 shows MAL conversion and MMA selectivity as functions of the reaction runs. The extent of the deactivation of catalyst was probed by employing the same catalyst sample in a number of reaction cycles. In Fig. 1, MAL conversion gradually decreased from 93.6% in the first run to 80.5% in the eighth run, and MMA selectivity remained constant except for the first run. The continuous decrease in MAL conversion indicated that the deactivation of the catalyst proceeded gradually. However, the increased selectivity observed in the second run was likely caused by the in situ formation of a Pd–H bond at 2034 cm^{-1} (shown in Fig. 2, proved by the Pd–H bond formed when the adsorption of H_2) for reduction of excess PdO_x and PbO_x in the catalyst and the production of bimetallic Pd_3Pb crystallites. The formation of Pd–H was by the chemical adsorption of methanol on the catalyst. As described in previous work [2,31], Pd_3Pb crystals were the active sites of reaction. The basic idea is that Pb^{2+} cannot be reduced to Pb^0 by an aqueous hydrazine solution on the surface of the support Al_2O_3 under ambient conditions; however, it can be readily reduced on the unsaturated Pd site to form bimetallic Pd_3Pb crystals.

3.2. Analysis of the fresh and degraded catalyst

To gain insight into the deactivation behavior of the $Pd_5Pb_5/MgO–Al_2O_3$ catalyst, the properties of the catalysts before

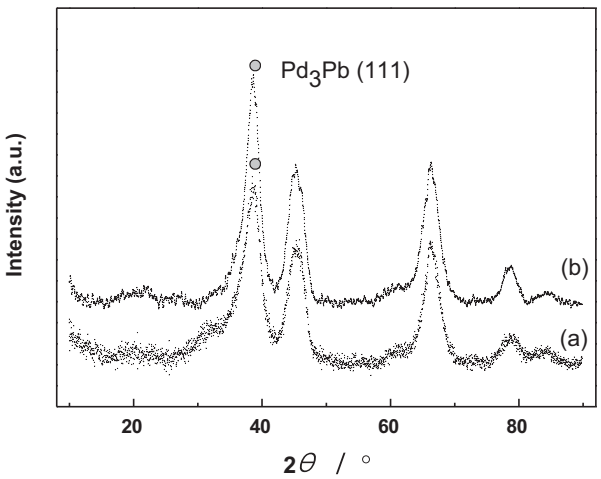

Fig. 3. XRD patterns of the fresh catalyst (a) and deactivated catalyst (b).

and after the tests were investigated through XRD, TEM, XPS, ICP-MS, BET and TG analysis.

3.2.1. XRD and TEM

The change in structure and the growth of a noble metal crystallite, which result in the loss of active surface area, are the main factors in the irreversible decrease of activity and the complete deactivation of noble metal catalysts. Generally, the change in the structure and the growth of a crystallite can be easily followed by XRD and TEM particle size measurement. The XRD measurements of the $Pd_5Pb_5/MgO–Al_2O_3$ catalysts before and after the test are shown in Fig. 3. The XRD pattern of the deactivated catalyst was similar to that of the fresh one, indicating that the deactivated catalyst remained in the original form after the direct oxidative esterification. The XRD pattern of the deactivated catalyst indicated that the well-defined face-center cubic structure of Pd_3Pb crystallite, corresponding to the diffraction at the 38.6° (1 1 1) plane, was not destroyed after eight runs. However, the intensity of the Pd_3Pb reflection peaks of the deactivated catalyst increased a little and full width at half maximum (FWHM) decreased (the wider the diffraction peak, the less intense the peak, and the smaller the crystal size). According to the results of Scherrer equation, the particle sizes of Pd_3Pb crystallites corresponds to the fresh catalyst was 5.3 nm, whereas particle sizes of Pd_3Pb crystallites corresponds to the deactivated catalyst was 5.6 nm. The particle sizes of the Pd_3Pb crystallites that corresponded to the fresh catalyst and the deactivated catalyst calculated with Scherrer equation were within the tolerance range of the calculated value; therefore, the particle sizes of the Pd_3Pb crystallites did not increase after usage.

The morphological change of noble metal entities because of particle growth by sintering or agglomeration is a major factor in catalyst deactivation [32–34]. In the study, agglomeration was partially prevented by the formation of Pd–H in the reaction. Fig. 4 shows TEM micrographs of the catalysts before and after the catalytic reaction. There were particles in the catalysts before and after the catalytic reaction. The size distributions of bimetallic Pd_3Pb crystals were all shown in Fig. 4. To calculate the size of the metal crystal, different areas were examined and about 200 crystals were counted. The growth of the Pd_3Pb crystallites induced by the reaction was minimal, from the previous average crystal size of 4.2 nm to typically 4.5 nm after eight-run reactions. The sizes of the Pd_3Pb crystallites in the fresh and deactivated catalysts calculated by Scherrer equation were a little larger than those calculated by TEM. TEM micrographs of the deactivated catalyst showed no

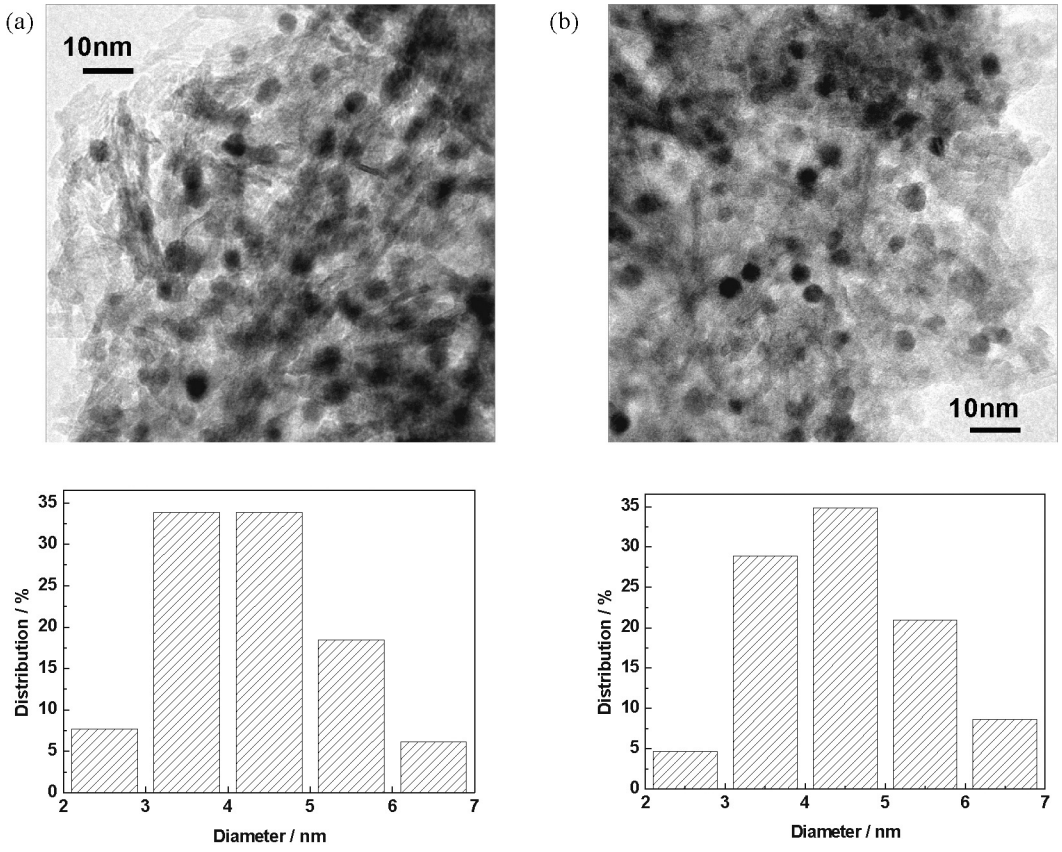

Fig. 4. TEM images and the size distributions of bimetallic Pd_3Pb crystals of the fresh catalyst (a) and deactivated catalyst (b).

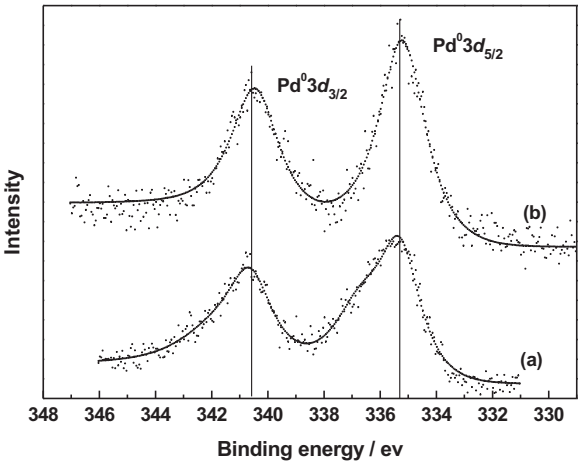

Fig. 5. XPS spectra of Pd 3d spectra of the fresh catalyst (a) and deactivated catalyst (b).

sintering and agglomeration of Pd_3Pb crystallites. The slight growth in the Pd_3Pb crystallites was not enough to conclude that it is the dominant factor in the deactivation.

3.2.2. XPS and ICP

In addition to structure change and particle growth, the valency change between PdO_x and metallic Pd may also be a prominent factor [35]. The changes in the chemical valency in the oxidation of a crystallite surface and the formation of too much Pd–H might synergistically affect the stability of the dispersion of the Pd_3Pb crystallites. Fig. 5 shows the Pd 3d spectra of the catalysts before and after the stability tests. The shoulder peak indicating PdO at about 337 eV was substantially decreased and the peak indicating zero-valent Pd of Pd_3Pb crystallites at 335 eV clearly increased, No oxidation of Pd_3Pb crystallites occurred with PdO_x, but there was a slight transformation of PdO_x to Pd_3Pb crystallites. The reduction of PdO to Pd_3Pb crystallites was favorable for the main reaction.

For metal catalysis, the leaching of metal atoms depends on the reaction medium (pH, oxidation potential, chelating properties of molecules) and surface metal properties [36]. In direct oxidative esterification with gas–liquid–solid phase in the atmosphere, the leaching of precious metal by formation of soluble complex compounds may occur. To prevent such occurrence, it is importance to avoid hydrogen-starving conditions and to keep the metallic Pd in a well-reduced metallic state. These results can be achieved by decreasing the partial pressure of oxygen in the reactor. Thus, the oxidation of bimetallic Pd_3Pb into PdO_x and PbO_x and the leaching of Pd are also decreased.

Table 1 provides the results of ICP-MS measurements of the Pd and Pb contents. The Pd content in the fresh catalyst was 4.9%, whereas the content was 4.5% in the used catalyst. Too much metal Pd was lost during the reaction. The leaching of the Pd metals seems to be the main factor in the deactivation. The results of the ICP-MS measurements of Pd and Pb contents in the solution shown in Table 2 are not consistent with the results of that in catalyst shown in Table 1. Very small amounts of Pd and Pb were detected in the solution sample after the reaction taken from the first and second batches. The content of Pd in the solution of the first batch was only 0.3 ppm and Pb was 11 ppm; in the eighth batch, the content of Pd was 0.1 ppm, whereas Pb was 9 ppm. The leaching of Pb was occurred because the weight loading of Pb on the catalyst exceeded the molar ratio of Pd to Pb in the Pd_3Pb crystallites [31]. The leaching content of Pd and Pb were about 6×10^{-4}% and 3×10^{-2}% in the fresh catalyst, which were calculated according to the mean value of Pd as 0.2 ppm and Pb as 10 ppm in each run. The very little content of Pd detected in the solution could not lead to the sharp decrease of the contents of Pd on the catalyst. The Pd content in the deactivated catalyst analyzed by ICP-MS is lower, the plausible explanation is that the weight of the organic substances adsorbed on the surface active sites of the catalyst, affected the calculation of the relative content of Pd and caused the content of Pd in the catalyst to become low. The very small amount of Pd detected in the solution could not lead to the sharp decrease of the catalytic activity, leaching should be not the dominant factor for the deactivation. To confirm whether the absorption of organic substances was the dominant factor in the deactivation, the fresh and deactivated catalysts were analyzed by BET and TG.

Table 1
ICP-MS measurements of Pd and Pb contents in the fresh and deactivated catalysts.

Catalyst	Pd (wt.%)	Pb (wt.%)
Fresh catalyst	4.9	4.9
Deactivated catalyst	4.5	4.4

Table 2
ICP-MS measurements of Pd and Pb contents in the solution.

Content	Pd (ppm)	Pb (ppm)
In the first batch	0.3	11
In the eight batch	0.1	9

3.2.3. BET and TG

The specific surface area, the pore volume (V_P) and the average pore size of the catalysts before and after the stability tests are summarized in Table 3. The S_{BET}, D_P, and V_P values for the catalyst after the stability test obviously decreased from 309.6 $m^2\ g^{-1}$, 8.0 nm, and 0.62 $cm^3\ g^{-1}$ to 255.5 $m^2\ g^{-1}$, 7.7 nm, and 0.50 $cm^3\ g^{-1}$. Thus, it could be estimated that about 20 vol.% of the pore volumes decreased. Similar deductions could be made from the differences in surface areas and the pore size distribution. The small surface areas and pore volumes of the deactivated catalyst indicated the accumulation of organic substances such as the polymer of methacrolein or methyl methacrylate. The polymeric or oligomeric species formed in the liquid phase tend to deposit on the surface of the heterogeneous catalysts and restrict the reactant access and product desorption. Even oligomers with small molecular weight are able to block pore entrance or restrict considerably the reactant diffusion toward metal particles [36]. The acid sites in the

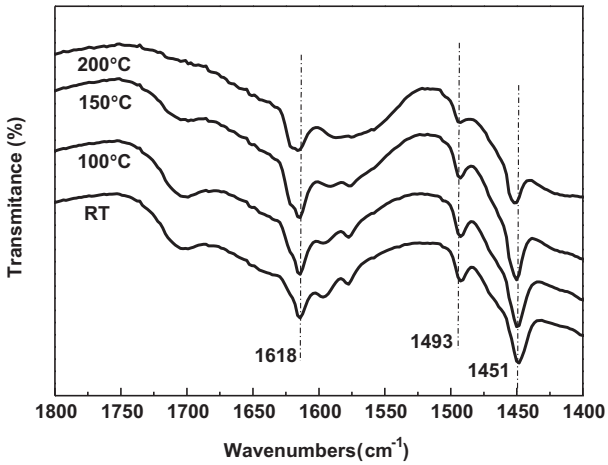

Fig. 6. FTIR spectra of pyridine adsorbed on $MgO–Al_2O_3$.

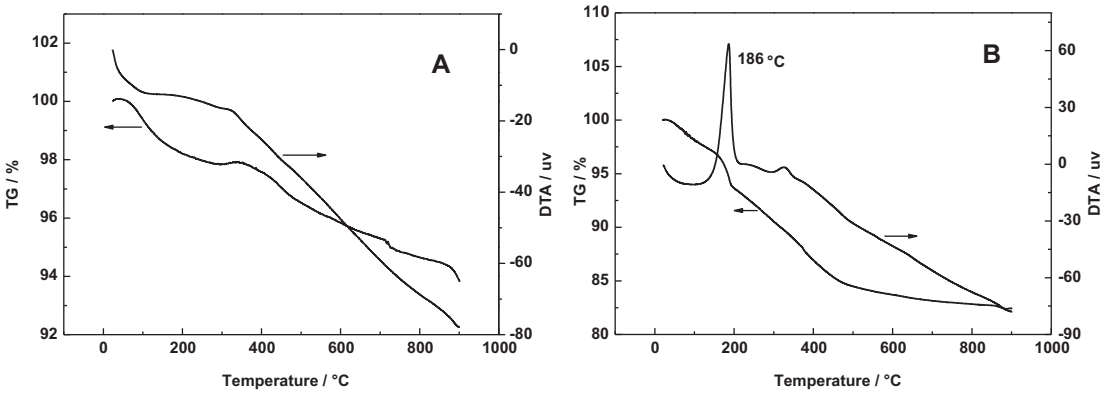

Fig. 7. TG/DTA curves of fresh catalyst (A) and deactivated catalyst (B) at a heating rate of 10 °C min^{-1} under air.

Table 3
Specific surface area, specific pore volume and average pore diameter of the fresh catalyst, deactivated catalyst and regenerated catalyst by washing with MeOH.

Catalyst	Specific surface area ($m^2\ g^{-1}$)	Specific pore volume ($cm^3\ g^{-1}$)	Average pore diameter (nm)
Fresh catalyst	309.6	0.62	8.0
Deactivated catalyst	255.5	0.50	7.7
Regenerated catalyst	303.6	0.60	8.0

$MgO–Al_2O_3$ support and heating lead to the dimolecular and multimolecular polymerization of the monomer MAL and MMA. The acid properties of support $MgO–Al_2O_3$ were examined by FT-IR spectroscopy with the pyridine adsorption technique, the spectrum of the physisorbed pyridine at ambient temperature and the following spectra obtained after evacuation at increasing temperature are shown in Fig. 6. Several bands were observed at around 1618 cm^{-1}, 1493 cm^{-1}, 1451 cm^{-1} and in the region from 1800 cm^{-1} to 1400 cm^{-1}. The IR bands at 1450 cm^{-1} are assigned to the pyridine adsorbed on Lewis acid sites, 1618 cm^{-1} is assigned to pyridine adsorbed with hydrogen bonding, and the IR band at 1493 cm^{-1} is attributed to both Brønsted and Lewis acid sites.

The accumulation of organic substances on the surface active sites of the catalyst after the stability tests was also evaluated through TG/DTA (heating rate of 10 °C min^{-1}) as shown in Fig. 7. From the room temperature up to 900 °C, the weight loss for the fresh catalyst was 6%; and the weight loss for the catalysts after the stability tests was 18%. DTA curves also showed the release of organic compounds. Consequently, the results of TG and BET confirmed that the Pd content of deactivated catalyst was lower than the actual content. Based on the analysis of TG and BET, the adsorption of polymers and some other organic substances was the primary reason in the deactivation of catalyst.

3.3. Reactivating the degraded catalyst

The deactivated catalyst can be regenerated in many methods. The adsorbed substances in the catalyst could be desorbed by washing the deactivated catalyst [28,36–41], which would result in the reactivation of the deactivated catalyst. The deactivated catalyst after the long-term reaction test (shown in Fig. 1) was washed by stirring in either MeOH or an aqueous hydrazine solution at the reaction temperature of 80 °C for 10 h. A new direct oxidative esterification of MAL with MeOH over the regenerated catalyst in the atmosphere was then carried out in batch process (shown in Fig. 8). The results in Fig. 8 indicated that washing the deactivated catalyst with either MeOH or an aqueous hydrazine solution could completely recover its activity, signifying that washing was effective in extracting the substances adsorbed on the catalyst. The activity and selectivity of the regenerated catalyst were a little higher than that of the fresh catalyst, which is likely due to the formation of Pd–H by the in situ reduction of PdO_x

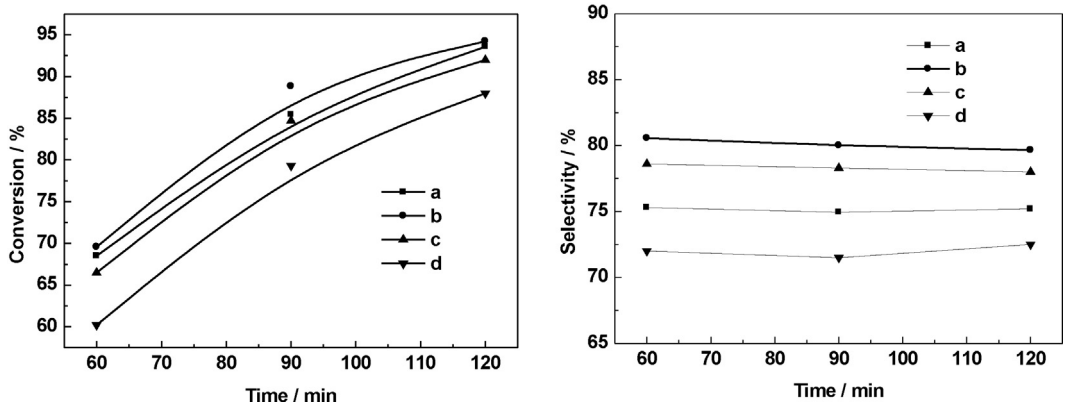

Fig. 8. Batch process of the direct oxidative esterification over the fresh catalyst (a), the regenerated catalyst by washing with MeOH (b) and an aqueous hydrazine solution (c), and the regenerated catalyst by calcining in air at 500 °C and reducing in an aqueous hydrazine solution (d).

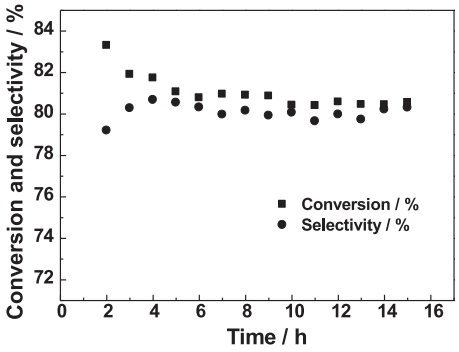

Fig. 9. Continuous-flow process of the direct oxidative esterification of MAL with MeOH over the regenerated catalyst by washing with MeOH.

and PbO_x to bimetallic Pd_3Pb crystallites under working conditions. The catalytic activity was completely recovered despite the loss of metal during the repeated reaction. The regeneration scheme that we used is considerably simple and practical. Regenerating the deactivated catalyst by washing with MeOH was more simple and practical than washing it with an aqueous hydrazine solution because MeOH is the reactant. The BET analysis of the regenerated catalyst washed with MeOH is shown in Table 3. The S_{BET}, D_P, and V_P values for the regenerated catalysts obviously increased to 303.6 $m^2\ g^{-1}$, 8.0 nm, and 0.60 $cm^3\ g^{-1}$ respectively.

The deactivated catalyst was also regenerated by calcination [42–44] in air at 500 °C and then reduced in an aqueous hydrazine solution. The activity of the regenerated catalyst in the batch process is also shown in Fig. 8. However, this method could not completely recover catalyst activity due to the crystallite growth at the high temperature of 500 °C. According to the TG analysis, the adsorbed organic substances on the surface active sites of catalyst would not be completely desorbed if the calcining temperature was lower than 500 °C. A higher temperature would lead to the crystallite growth and oxidation of Pd_3Pb crystallites. From the analysis above, the regeneration scheme of washing with MeOH was practical and meaningful.

Fig. 9 shows the continuous-flow reaction of direct oxidative esterification of MAL with MeOH in the reaction atmosphere over the regenerated catalyst by washing with MeOH. There was no degradation of activity in the continuous-flow process, because the local excess of organic substances on the catalyst in batch process was avoided through the flow of MeOH in the continuous-flow process [28,45].

4. Conclusions

By combining the measurements of the reaction and deactivation process in direct oxidative esterification, as well as ex situ catalyst characterization before and after the reaction, we confirm that the $Pd_5Pb_5/MgO–Al_2O_3$ catalyst gradually deactivated during batch reaction. The factors in the deactivation and the regeneration of the degraded catalysts had been studied.

XRD, TEM, XPS and ICP-MS analysis demonstrated that the change of structure and leaching of the noble metal crystallite were not significant contributors to activity decline even through the definite loss of Pd and Pb. The result of TG analysis was consistent with that of Brunauer–Emmett–Teller method analysis. The explanation for the catalyst deactivation was the accumulation of organic substances (such as dimolecular and multimolecular polymerization of the monomers MAL and MMA) on the surface active sites of the catalyst.

Washing the deactivated catalyst with MeOH or an aqueous hydrazine solution at 80 °C for 10 h allowed the deactivated catalyst to completely recover its initial catalytic activity. The results suggested that the deactivation was mainly due to the accumulation of organic substances on the surface active sites. Calcination in air at 500 °C and then reduced in an aqueous hydrazine solution could also recover the partial activity of the catalyst. No distinct degradation of activity was observed in the continuous-flow reaction over the regenerated catalyst by stirring in MeOH. The analysis of the deactivation and regeneration of the catalyst is meaningful in the commercialization of this process.

Acknowledgements

Financial support for this work was provided by General Program Youth of National Natural Science Foundation of China (21006106), “Strategic Priority Research Program” of the Chinese Academy of Sciences (XDA07070600), and National High Technology Research and Development Program of China (863 Program) (2012AA062903).

References

[1] K. Nagai, Applied Catalysis A 221 (2001) 367.
[2] T. Miyakea, T. Asakawa, Applied Catalysis A 280 (2005) 47.
[3] M. Takeshi, Y. Tatsuo, JP Patent 2002241345 (2002); to Aashi Chemical Corp.
[4] Y. Koushirou, Y. Tatsuo, W. Toru, JP Patent 2003267928 (2003); to Aashi Chemical Corp.
[5] W. Zhao, W.G. Cheng, Z.X. Li, L. Wang, X.P. Zhang, S.J. Zhang, Chinese Chemical Letters 17 (2006) 739–742.
[6] H.F. Dong, Z.X. Li, Z.P. Wang, W. Zhao, Y.Y. Diao, S.J. Zhang, Chinese Journal of Process Engineering 6 (2006) 661–665.
[7] H.F. Dong, Z.X. Li, Z.P. Wang, W.G. Cheng, W. Zhao, X.P. Zhang, S.J. Zhang, Chinese Journal of Chemical Industry and Engineering 57 (2006) 1346–1350.
[8] Y. Tatsuo, M. Takeshi, A. Kenji, JP Patent 2007297224 (2007); to Aashi Chemical Corp.
[9] A. Baylet, S. Royer, P. Marécot, J.M. Tatibouët, D. Duprez, Applied Catalysis B 77 (2008) 237–247.
[10] M.D. Hernández-Alonso, I. Tejedor-Tejedor, J.M. Coronado, M.A. Anderson, Applied Catalysis B 101 (2011) 283–293.
[11] S. Brandenberger, O. Kröcher, M. Casapu, A. Tissler, R. Althoff, Applied Catalysis B 101 (2011) 649–659.
[12] I. Sierra, J. Ereña, A.T. Aguayo, J.M. Arandes, M. Olazar, J. Bilbao, Applied Catalysis B 106 (2011) 167–173.
[13] C.A. Franchini, A.M. Duarte de Farias, E.M. Albuquerque, R. Santos, M.A. Fraga, Applied Catalysis B 117/118 (2012) 302–309.
[14] F. Wang, W. Cai, Tana, H. Provendier, Y. Schuurman, C. Descorme, C. Mirodatos, W. Shen, Applied Catalysis B 125 (2012) 546–555.
[15] T.F. Garetto, C.I. Vignatti, A. Borgna, A. Monzón, Applied Catalysis B 87 (2009) 211–219.
[16] A. Simson, R. Farrauto, M. Castaldi, Applied Catalysis B 106 (2011) 295–303.
[17] S. Lee, G. Keskar, C. Liu, W.R. Schwartz, C.S. McEnally, J.Y. Kim, L.D. Pfefferle, G.L. Haller, Applied Catalysis B 111/112 (2012) 157–164.
[18] D.E. Doronkin, T.S. Khan, T.B.S. Fogel, P. Gabrielsson, S. Dahl, Applied Catalysis B 117/118 (2012) 49–58.
[19] H.Y. Fan, C. Shi, X.S. Li, S. Zhang, J.L. Liu, A.M. Zhu, Applied Catalysis B 119/120 (2012) 49–55.
[20] P. Konova, A. Naydenov, C. Venkov, D. Mehandjiev, D. Andreeva, T. Tabakova, Journal of Molecular Catalysis A 213 (2004) 235–240.
[21] G. Elordi, M. Olazar, G. Lopez, P. Castaño, J. Bilbao, Applied Catalysis B 102 (2011) 224–231.
[22] E. López, S. Ordóñez, F.V. Díez, Applied Catalysis B 62 (2006) 57–65.
[23] J.H. Lee, L.D. Trimm, Fuel Processing Technology 42 (1995) 339–359.
[24] H. Ohtsuka, T. Tabata, Applied Catalysis B 21 (1999) 133–139.
[25] M.A. Aramendía, R. Burch, I.M. García, A. Marinas, J.M. Marinas, B.W.L. Southward, F.J. Urbano, Applied Catalysis B 31 (2001) 163–171.
[26] D. Meloni, R. Monaci, Z. Zedde, M.G. Cutrufello, S. Fiorilli, I. Ferino, Applied Catalysis B 102 (2011) 505–514.
[27] Y.C. Lin, K.L. Hohn, S.M. Stagg-Williams, Applied Catalysis A 327 (2007) 164–172.
[28] N.C. Concibido, T. Okuda, W. Nishijima, M. Okada, Applied Catalysis B 71 (2007) 64–69.
[29] V. Narayana Kalevaru, A. Benhmid, J. Radnik, M.M. Pohl, U. Bentrup, A. Martin, Journal of Catalysis 246 (2007) 399–412.
[30] C.E. Volckmar, M. Brona, U. Bentrup, A. Martin, P. Claus, Journal of Catalysis 261 (2009) 1–8.
[31] Y.Y. Diao, R.Y. Yan, S.J. Zhang, P. Yang, Z.X. Li, L. Wang, H.F. Dong, Journal of Molecular Catalysis A 303 (2009) 35–42.

[32] H. Hashimoto, Z.M. Sun, S. Tada, Journal of Alloys and Compounds 441 (2007) 174–180.
[33] K. Narui, H. Yata, K. Furuta, A. Nishida, Y. Kohtoku, T. Matsuzaki, Applied Catalysis A 179 (1999) 165–173.
[34] E. Czerwosza, P. Dluzewskic, M. Kozlowskib, M. Nowickid, A. Richtere, Vacuum 74 (2004) 311–315.
[35] P. Euzen, J.H. Le Gal, B. Rebours, G. Martin, Catalysis Today 47 (1999) 19–27.
[36] R. Khodayari, C.U. Ingemar Odenbrand, Applied Catalysis B 33 (2001) 277–291.
[37] M. Besson, P. Gallezot, Catalysis Today 81 (2003) 547–559.
[38] G. Yuan, M.A. Keane, Catalysis Today 88 (2003) 27–36.
[39] W.H. Wu, J. Xu, R. Ohnishi, Applied Catalysis B 60 (2005) 129–137.
[40] O. Akdim, U.B. Demirci, P. Miele, International Journal of Hydrogen Energy 36 (2011) 13669–13675.
[41] G.M. Arzac, D. Hufschmidt, M.C. Jiménez De Haro, A. Fernández, B. Sarmiento, M.A. Jiménez, M.M. Jiménez, International Journal of Hydrogen Energy 37 (2012) 14373–14381.
[42] O. Ilinich, W. Ruettinger, X. Liu, R. Farrauto, Journal of Catalysis 247 (2007) 112–118.
[43] D.S. Mao, G.Z. Lu, Q.L. Chen, Journal of Molecular Catalysis A 240 (2005) 164–171.
[44] H. Liu, G.Z. Lu, Y.L. Guo, Y. Guo, J.S. Wang, Chemical Engineering Journal 108 (2005) 187–192.
[45] F.J. Urbano, J.M. Marinas, Journal of Molecular Catalysis A 173 (2001) 329–345.